

Quantum Optimal Control for Coherent Spin Dynamics of Radical Pairs via Pontryagin Maximum Principle

U. G. Abdulla^{1,*}, J. H. Rodrigues¹, and J. -J. Slotine²

¹*Okinawa Institute of Science and Technology 1919-1 Tancha,
Onna-son, Kunigami-gun Okinawa, Japan 904-0495 and*

²*Nonlinear Systems Laboratory, Department of Mechanical Engineering,
Massachusetts Institute of Technology, Cambridge, Massachusetts, USA*

(Dated: August 5, 2025)

Abstract

This paper aims at devising the shape of the external electromagnetic field which drives the spin dynamics of radical pairs to quantum coherent state through maximization of the triplet-singlet yield in biochemical reactions. The model is a Schrödinger system with spin Hamiltonians given by the sum of Zeeman interaction and hyperfine coupling interaction terms. We introduce a one-parameter family of optimal control problems by coupling the Schrödinger system to a control field through filtering equations for the electromagnetic field. Fréchet differentiability and the Pontryagin Maximum Principle in Hilbert space is proved, and the bang-bang structure of the optimal control is established. A new iterative Pontryagin Maximum Principle (IPMP) method for the identification of the bang-bang optimal control is developed. Numerical simulations based on IPMP and the gradient projection method (GPM) in Hilbert spaces are pursued, and the convergence, stability and the regularization effect are demonstrated. Comparative analysis of filtering with regular optimal electromagnetic field versus non-filtering with bang-bang optimal field (*Abdulla et al, Quantum Sci. Technol.*, **9**, 4, 2024) demonstrates the change of the maxima of the singlet yield is less than 1%. The results open a venue for a potential experimental work for the magnetoreception as a manifestation of quantum biological phenomena.

I. INTRODUCTION

One of the great challenges of modern science is to bridge the gap between atomic and cellular level phenomena that determine the condition and outcomes of our cells. Quantum biology is an emerging field with the aim to comprehend quantum effects in biochemical mechanisms and biological function [1–3]. The field of quantum biology currently focuses on several areas of research: photosynthesis, and magnetoreception [4–10]; olfaction [11, 12]; enzymatic activity, fruit fly navigation, ATP production, and vision [13–19]. However, it should be mentioned that there is no clear consensus on the presence of genuine quantum mechanical effects in biology, e.g. in avian magnetoreception and photosynthesis there are other proposed mechanisms such as navigation using a magnetite-based mechanism [20, 21]. In [22] quantum coherence effects that control the biological production of specific reactive oxygen species (ROS) in mammalian cells is presented. ROS balance is known to affect

* Ugur.Abdulla@oist.jp

cellular signaling, proliferation, and redox homeostasis [23–27]. Increased understanding of bio-physical and bio-molecular mechanisms that control specific ROS product channels, at the point of generation, may open new therapeutic avenues; particularly in neural-heightened medicine, enhanced wound healing, and improved human performance.

The spin-correlated radical-pair mechanism (SRPM) offers the best understood and established explanation of how magnetic fields might influence biochemical reactions [28, 29]. Magnetic field effects are possible during the singlet-triplet spin evolution of two radicals [30], which are in the same “cage” that form a radical pair. Applied magnetic fields can affect two main internal interactions of the radical pair whose time-dependences affect the temporal evolution of the singlet-triplet mixing, and thereby modulate relative reaction rates: electron-nuclear hyperfine interactions (HFI) and radical Zeeman (Δg) energies; both interactions have energies ($\sim 10^8 - 10^9$ rad/sec) much less than kT thermal energy (10^{13} rad/sec). SRPM is typically an adiabatic process, uncoupled to the thermal bath, therefore non-thermal effects of magnetic fields in biological systems are expected through these magnetic field and resonant frequency regimes without explicit influence of temperature. The effect of the HFI and Zeeman resonances are dependent on the frequency (resonant), strength, and orientation (relative to the molecular frame) of magnetic fields; these parameters can thus influence the relative reaction rates and product distributions of reactions of radical pairs. It is of great importance to identify magnetic field parameters to modulate quantum coherences in a radical pair reaction [8, 9, 31–33]. Here, we make the quantum coherence and singlet product yield indistinguishable.

In a broader context, the goal of this paper is to reveal the major mathematical principle of quantum optimal control theory (QOCT) and develop a roadmap leading straight to the experimental applications where a new generation of quantum technology is created on physical or biological systems serving as hardware platforms. The description and understanding of the mathematical principles of the QOCT is of fundamental importance for the development of a new generation of quantum technologies [34–38]. Some of the recent examples of successful application of QOCT methods in experiments for the development of a new generation of quantum technology are [39–45].

In [31] an optimization method that combines sensitivity analysis with Tikhonov regularization is implemented [46–49]. The numerical results of [31] demonstrated that the quantum singlet-triplet yield of the radical pair system can be significantly reduced if optimization

is simultaneously pursued for both external magnetic fields and internal hyperfine parameters. However, the method implemented in [31] is limited to constant-in-time magnetic field parameters.

In a recent paper [32] optimal control of the external electromagnetic field which maximize the quantum singlet-triplet yield of simplified radical pairs modeled by Schrödinger system with spin Hamiltonians given by the sum of Zeeman interaction and hyperfine coupling interaction terms are analyzed. Fréchet differentiability and Pontryagin Maximum Principle in Hilbert space setting is proved and bang-bang structure of the optimal control is established. Closed optimality system of nonlinear differential equations for the identification of the bang-bang optimal control is revealed and an effective numerical method for the identification of the bang-bang optimal magnetic field intensity for achieving a quantum coherence for the radical pair system is developed.

It is remarkable that the optimal magnetic pulse driving the complex quantum system to coherent state has a simple bang-bang structure. The Pontryagin Maximum Principle - a fundamental mathematical principle for the optimality of complex dynamical systems - turns out to be a fundamental principle for quantum coherence as well. Pontryagin Maximum Principle implies that along the optimal state and adjointed trajectories almost at every time instance the Hamilton-Pontryagin function achieves the maximum value with respect to finite-dimensional control parameter precisely at the value of the optimal control parameter. Due to the structure of the Hamilton-Pontryagin function, which inherited the structure of the Hamiltonian, its maximum with respect to each component of the control parameter is always achieved at the extreme values. Hence, the complex quantum system is driven to coherent state through banging of the components of the external magnetic pulse between its extreme values in specific time intervals.

Despite its great theoretical value and opening a venue for potential experimental applications in magnetoreception, the result raised a major technical question about how practical it will be to arrange a bang-bang electromagnetic wave in a short time scale.

Question: *What would be the simplest continuous in time electromagnetic wave input which is almost optimal in the sense that it provides a quantum triplet-singlet yield with minimal loss of the optimal one corresponding to optimal bang-bang electromagnetic field input?*

To answer this question we introduce an idea of coupling the Schrödinger system to a

control field through the first order filtering ordinary differential equation (ODE) for the electromagnetic field. We prove Pontryagin Maximum Principle and bang-bang structure of the optimal control. Therefore, an optimal electromagnetic field intensity becomes the solution of the filtering ODE with bang-bang input. Accordingly, optimal electromagnetic field intensity is continuous and piecewise-smooth in time. We implement a novel iterative PMP method for the numerical solution of the filtered optimal control problem. Comparative analysis of filtering with regular optimal electromagnetic field versus non-filtering with bang-bang optimal field [32] demonstrates the change of the maxima of the triplet-singlet yield is less than 1%. The approach is numerically effective and significantly simpler than existing methods for finite bandwidth input approximations, e.g. such as those based on Fourier decompositions [50].

The organization of the paper is as follows. In Section II the mathematical model of the spin dynamics of radical pairs is described. In Section III optimal control problem is formulated. Main results on the Fréchet differentiability of the quantum singlet yield, formula for the first-order Fréchet derivative, and the necessary condition for the optimality are presented in Section IV. In Section V we prove Pontryagin Maximum Principle and establish a bang-bang structure of the optimal control. We derive an optimal control synthesizing function by expressing optimal control through optimal and adjoint trajectories. The latter implies the closed nonlinear optimality system for the identification of the bang-bang optimal control. Section VI outlines gradient projection method (GPM) in Hilbert space, and iterative Pontryagin Maximum Principle (IPMP) algorithm for the identification of the bang-bang optimal control. Numerical results for the calculation of the bang-bang optimal control and continuous in time optimal electromagnetic field based on the GPM and IPMP algorithms are presented in Section VII. The main conclusions are outlined in Section VIII.

II. MATHEMATICAL MODEL

We consider the spin dynamics of correlated radical pair system obtained from triplet born states governed by the *filtered Schrödinger system*

$$i\hbar \frac{d\psi^l}{dt} = \mathbf{H}(\mathbf{v})\psi^l, \quad \text{in } (0, T], \quad \psi^l(0) = \psi_T^l, \quad l = 1, \dots, s, \quad (1)$$

$$\frac{d\mathbf{v}}{dt} + \gamma\mathbf{v} = \gamma\mathbf{u}, \quad \text{in } (0, T]; \quad \mathbf{v}(0) = \mathbf{v}_0, \quad (2)$$

where \hbar is the Plank constant, $\psi^l : [0, T] \rightarrow \mathbb{C}^n$ is the state vector, $\mathbf{H} : \mathbb{R}^3 \rightarrow \mathbb{C}^{n \times n}$ is the Hamiltonian operator, $\psi_T^l \in \mathbb{C}^n$ is the triplet state, $s \in \mathbb{N}$ is the number of triplet states, $\mathbf{v} \in L_2^3(0, T; \mathbb{R}^3)$ is the magnetic field vector function, $\gamma > 0$ be a filtration parameter, $\mathbf{v}_0 \in \mathbb{R}^3$ and $\mathbf{u} \in L_2^3(0, T; \mathbb{R}^3)$ be a control parameter. For the $p \in \mathbb{N}$ proton model with 1/2-spin, the number of triplet states is $3 \cdot 2^p$, and the state dimension is $n = 2^{p+2}$. The triplet states can be classified as follows:

$$\text{T0 states: } \psi_T^{j-2^p} = \frac{e_j - e_{j+2^p}}{\sqrt{2}}, j = 2^p + 1, \dots, 2^{p+1};$$

$$\text{T+ states: } \psi_T^j = e_{j-2^p}, j = 2^p + 1, \dots, 2^{p+1};$$

$$\text{T- states: } \psi_T^j = e_{j+2^p}, j = 2^{p+1} + 1, \dots, 3 \cdot 2^p,$$

where we use a notation $\{e_j\}$ for the standard orthonormal basis in \mathbb{R}^n . Spin Hamiltonian \mathbf{H} is given as a sum of three terms

$$\mathbf{H}(\mathbf{v}) = \mathbf{H}_Z(\mathbf{v}) + \mathbf{H}_{hfi} - i\mathbf{K}. \quad (3)$$

where

$$\mathbf{H}_Z(\mathbf{v}) = \mu_B g [(S_{1x} + S_{2x})v_x + (S_{1y} + S_{2y})v_y + (S_{1z} + S_{2z})v_z], \quad (4)$$

be a Zeeman interaction term with

$$\mathbf{v} = \mathbf{v}(t) = (v_x(t), v_y(t), v_z(t)) \in C(0, T; \mathbb{R}^3),$$

where the constants μ_B and g stand for the Bohr's magneton and the electron's spin ratio, and $S_1 = (S_{1i})_{i=x,y,z}$ and $S_2 = (S_{2i})_{i=x,y,z}$ are the electron's spin operators. The static Hermitian operators \mathbf{H}_{hfi} and \mathbf{K} are defined as

$$\mathbf{H}_{hfi} = \mu_B g \sum_{j=1}^p \sum_{i=x,y,z} A_{ji} I_{ji} S_{1i}, \quad \mathbf{K} = \frac{1}{2} (k_S P_S + k_T P_T) \quad (5)$$

where $A_j = (A_{ji})_{i=x,y,z} \in \mathbb{R}^3$ is the hyperfine parameters corresponding to the j -proton, and $I_j = (I_{ji})_{i=x,y,z}$ is the corresponding nucleus spin operator, for $j = 1, \dots, p$. Finally, $k_S, k_T > 0$ are diffusion rates, and P_S and P_T are the projection operators onto singlet and triplet states, respectively. For the particular case $p = 1$, electrons and nucleus spin

operators are given below

$$\begin{aligned} S_1 &= \left(\frac{1}{2}\sigma_x \otimes E_2 \otimes E_2, \frac{1}{2}\sigma_y \otimes E_2 \otimes E_2, \frac{1}{2}\sigma_z \otimes E_2 \otimes E_2 \right); \\ S_2 &= \left(E_2 \otimes \frac{1}{2}\sigma_x \otimes E_2, E_2 \otimes \frac{1}{2}\sigma_y \otimes E_2, E_2 \otimes \frac{1}{2}\sigma_z \otimes E_2 \right); \\ I_1 &= \left(E_2 \otimes E_2 \otimes \frac{1}{2}\sigma_x, E_2 \otimes E_2 \otimes \frac{1}{2}\sigma_y, E_2 \otimes E_2 \otimes \frac{1}{2}\sigma_z \right), \end{aligned}$$

where E_2 is the identity matrix of order 2, and σ_i , $i = x, y, z$ denotes the Pauli matrices. In addition to this case, the projection operators are defined as

$$P_S = \frac{1}{3}E_8 - S_1 \cdot S_2, \quad P_T = \frac{3}{4}E_8 + S_1 \cdot S_2,$$

where E_8 denotes the identity matrix of order 8.

A. First Order Filtering

Given $\gamma > 0$, $\mathbf{v}_0 \in \mathbb{R}^3$ and $\mathbf{u} \in L_2^3(0, T; \mathbb{R}^3)$, the *filtering equation* (2) provides continuous in time electromagnetic field intensity according to the formula

$$\mathbf{v}(t; \mathbf{u}) = e^{-\gamma t} \left[\mathbf{v}_0 + \int_0^t \gamma e^{\gamma \tau} \mathbf{u}(\tau) d\tau \right], \quad t \in [0, T]. \quad (6)$$

III. OPTIMAL CONTROL PROBLEM

Consider the optimal control problem of maximizing the amount of triplet born singlet yield over the time interval $[0, T]$

$$\mathcal{J}(\mathbf{u}) = \frac{k_S}{3 \cdot 2^{p+1}} \sum_{l=1}^{3 \cdot 2^p} \int_0^T \langle \psi^l(t; \mathbf{u}) | P_S | \psi^l(t; \mathbf{u}) \rangle_{\mathbb{C}^n} dt \rightarrow \max \quad (7)$$

on a control set

$$\mathcal{V} = \left\{ \mathbf{u} \in L_2^3(0, T; \mathbb{R}^3) : \mathbf{u}(t) \in V = \prod_{i=x,y,z} [m_i, M_i] \text{ for a.e. } t \in [0, T] \right\} \quad (8)$$

where $\left((\psi^l(t; \mathbf{u}))_{l=1}^{3 \cdot 2^p}, \mathbf{v}(t; \mathbf{u}) \right)$ is the corresponding solution of the filtered Schrödinger system (1),(2).

IV. FRÉCHET DIFFERENTIABILITY AND PONTRYAGIN MAXIMUM PRINCIPLE

Define the *Hamilton Pontryagin function*

$$\begin{aligned}\mathcal{H}(\psi(t), \mathbf{u}(t), \chi(t)) &:= \mathcal{H}(\psi, \mathbf{u}, \chi)(t) \\ &= \frac{\mu_B g}{3 \cdot 2^{p-1}} \sum_{l=1}^{3 \cdot 2^p} \int_t^T \text{Im} \langle \chi^l(\tau) | \mathbf{S}_1 + \mathbf{S}_2 | \psi^l(\tau) \rangle_{\mathbb{C}^n} \gamma e^{\gamma(t-\tau)} d\tau \cdot \mathbf{u}(t),\end{aligned}\quad (9)$$

where $\psi^l, \chi^l : [0, T] \rightarrow \mathbb{C}^n$, $l = 1, \dots, 3 \cdot 2^p$ and $\mathbf{u} : [0, T] \rightarrow \mathbb{R}^3$.

The following is the Fréchet differentiability result of the cost functional \mathcal{J} .

Theorem 1 *The functional \mathcal{J} is continuously differentiable in \mathcal{V} , and the Fréchet derivative $\mathcal{J}'(\mathbf{u}) \in L_2^3(0, T; \mathbb{R}^3)$, for $\mathbf{u} \in \mathcal{V}$, is given by*

$$\mathcal{J}'(\mathbf{u}) = \frac{\partial \mathcal{H}}{\partial \mathbf{u}} = \frac{\gamma \mu_B g}{3 \cdot 2^{p-1}} \sum_{l=1}^{3 \cdot 2^p} \int_t^T \text{Im} \langle \chi^l(\tau; \mathbf{u}) | S_1 + S_2 | \psi^l(\tau; \mathbf{u}) \rangle_{\mathbb{C}^n} e^{\gamma(t-\tau)} d\tau, \quad (10)$$

where $\left((\psi^l(t; \mathbf{u}))_{l=1}^{3 \cdot 2^p}, \mathbf{v}(t; \mathbf{u}) \right)$ is the solution of (1), (2) and $(\chi^l(\cdot; \mathbf{u}))_{l=1}^{3 \cdot 2^p}$ be a solution of the corresponding adjoint Schrödinger system

$$i\hbar \frac{d\chi^l}{dt} = \mathbf{H}^*(\mathbf{v})\chi^l - i\frac{k_S}{2} P_S \psi^l, \quad \text{in } [0, T]; \quad \chi^l(T) = 0, \quad (11)$$

where

$$\mathbf{H}^*(\mathbf{v}) = \mathbf{H}_z(\mathbf{v}) + \mathbf{H}_{hfi} + i\mathbf{K}. \quad (12)$$

be an adjoint Hamiltonian.

Proof. Let $\mathbf{u} \in \mathcal{V}$ and consider an increment $\delta \mathbf{u} \in L_2^3(0, T; \mathbb{R}^3)$ such that $\mathbf{u} + \delta \mathbf{u} \in \mathcal{V}$. Denote $\psi^l = \psi^l(\cdot; \mathbf{u})$ and $\bar{\psi}^l = \bar{\psi}^l(\cdot; \mathbf{u} + \delta \mathbf{u})$ the corresponding solutions of (1) with $\psi_T = \psi_T^l$, $l = 1, \dots, 3 \cdot 2^m$. The vector-functions $\delta \psi^l = \bar{\psi}^l - \psi^l$ and $\delta \mathbf{v}$ is a solution of the Cauchy problem:

$$i\hbar \frac{d\delta \psi^l}{dt} = \mathbf{H}(\mathbf{v})\delta \psi^l + \mathbf{H}_z(\delta \mathbf{v})\bar{\psi}^l, \quad 0 \leq t \leq T; \quad \delta \psi^l(0) = 0 \quad (13)$$

$$\frac{d\delta \mathbf{v}}{dt} + \gamma \delta \mathbf{v} = \gamma \delta \mathbf{u}, \quad 0 \leq t \leq T; \quad \delta \mathbf{v}(0) = 0 \quad (14)$$

or, equivalently the pair $(\delta \psi^l, \delta \mathbf{v})$ solves the integral equation in $(0, T)$:

$$\delta \psi^l(t) = -i\hbar^{-1} \int_0^t \mathbf{H}(\mathbf{v}(\tau))\delta \psi^l(\tau) d\tau - i\hbar^{-1} \int_0^t \mathbf{H}_z(\delta \mathbf{v}(\tau))\bar{\psi}^l(\tau) d\tau, \quad (15)$$

$$\delta \mathbf{v}(t) = \int_0^t \gamma e^{\gamma(\tau-t)} \delta \mathbf{u}(\tau) d\tau. \quad (16)$$

From (6),(15),(16) it follows that

$$|\mathbf{v}(t)| \leq C, \quad |\delta \mathbf{v}(t)| \leq C \int_0^t |\delta \mathbf{u}(\tau)| d\tau, \quad (17)$$

$$|\delta \psi^l(t)| \leq C \int_0^t |\mathbf{v}(\tau)| |\delta \psi^l(\tau)| d\tau + C \int_0^t |\delta \mathbf{v}(\tau)| d\tau, \quad (18)$$

for $0 \leq t \leq T$. Since $\mathbf{u} \in \mathcal{V}$, it follows that

$$|\delta \psi^l(t)| \leq C_1 \int_0^t |\delta \psi^l(\tau)| d\tau + C \int_0^t |\delta \mathbf{u}(\tau)| d\tau, \quad 0 \leq t \leq T. \quad (19)$$

Using Gronwall's lemma [51] from (19) it follows that

$$|\delta \psi^l(t)| \leq C e^{C_1 T} \int_0^T |\delta \mathbf{u}(\tau)| d\tau, \quad 0 \leq t \leq T. \quad (20)$$

Note, that similarly we can establish a uniform boundedness of the state and adjoined vectors. Given $\mathbf{u} \in \mathcal{V}$, the state vector ψ^l , and adjoined vector χ^l satisfy the following integral equations:

$$\begin{aligned} \psi^l(t) &= -i\hbar^{-1} \int_0^t \mathbf{H}(\mathbf{v}(\tau)) \psi^l(\tau) d\tau + \psi_T^l, \\ \chi^l(t) &= \int_t^T i \left[\hbar^{-1} \mathbf{H}^*(\mathbf{v}(\tau)) \chi^l(\tau) + \frac{k_S}{2\hbar} \mathbf{P}_S \psi^l(\tau) \right] d\tau, \end{aligned}$$

where \mathbf{v} satisfies (6). Applying Gronwall's lemma again, we derive the uniform bound

$$\max(|\psi^l(t)|, |\chi^l(t)|) \leq C, \quad 0 \leq t \leq T, \quad (21)$$

where the constant C depends on T, m_i, M_i .

Next, we transform an increment of the functional (7) as follows:

$$\begin{aligned} &\mathcal{J}(\mathbf{u} + \delta \mathbf{u}) - \mathcal{J}(\mathbf{u}) \\ &= \frac{k_S}{3 \cdot 2^p} \sum_{l=1}^{3 \cdot 2^p} \int_0^T \left[\operatorname{Re} \langle \psi^l(t) | P_S | \delta \psi^l(t) \rangle_{\mathbb{C}^n} + \frac{1}{2} \langle \delta \psi^l(t) | P_S | \delta \psi^l(t) \rangle_{\mathbb{C}^n} \right] dt, \end{aligned} \quad (22)$$

where $\delta \psi^l = \bar{\psi}^l - \psi^l$. Using (11),(13) we have

$$\begin{aligned} 0 &= \int_0^T i\hbar \frac{d}{dt} \langle \chi^l | \delta \psi^l \rangle_{\mathbb{C}^n} dt = \int_0^T \left[\langle -i\hbar \frac{d\chi^l}{dt} | \delta \psi^l \rangle_{\mathbb{C}^n} + \langle \chi^l | i\hbar \frac{d\delta \psi^l}{dt} \rangle_{\mathbb{C}^n} \right] dt \\ &= \int_0^T \left[\langle -\mathbf{H}^*(\mathbf{v}) \chi^l | \delta \psi^l \rangle_{\mathbb{C}^n} + \langle \chi^l | \mathbf{H}(\mathbf{v}) \delta \psi^l \rangle_{\mathbb{C}^n} \right] - \int_0^T i \frac{k_S}{2} \langle \psi^l | P_S | \delta \psi^l \rangle_{\mathbb{C}^n} dt \\ &\quad + \int_0^T \langle \chi^l | \mathbf{H}_z(\delta \mathbf{v}) | \psi^l \rangle_{\mathbb{C}^n} + \langle \chi^l | \mathbf{H}_z(\delta \mathbf{v}) | \delta \psi^l \rangle_{\mathbb{C}^n} dt \end{aligned}$$

which implies

$$\frac{k_S}{2} \int_0^T \operatorname{Re} \langle \psi^l | P_S | \delta \psi^l \rangle_{\mathbb{C}^n} = \int_0^T \operatorname{Im} \langle \chi^l | \mathbf{H}_z(\delta \mathbf{v}) | \psi^l \rangle_{\mathbb{C}^n} dt + \int_0^T \operatorname{Im} \langle \chi^l | \mathbf{H}_z(\delta \mathbf{v}) | \delta \psi^l \rangle_{\mathbb{C}^n} dt. \quad (23)$$

Combining (22) and (23) we obtain

$$\mathcal{J}(\mathbf{u} + \delta \mathbf{u}) - \mathcal{J}(\mathbf{u}) = \frac{1}{3 \cdot 2^{p-1}} \sum_{l=1}^{3 \cdot 2^p} \int_0^T \operatorname{Im} \langle \chi^l | \mathbf{H}_z(\delta \mathbf{v}) | \psi^l \rangle_{\mathbb{C}^n} dt + R, \quad (24)$$

where

$$R = \frac{1}{3 \cdot 2^p} \sum_{l=1}^{3 \cdot 2^p} \int_0^T \left[2 \operatorname{Im} \langle \chi^l | \mathbf{H}_z(\delta \mathbf{v}) | \delta \psi^l \rangle_{\mathbb{C}^n} + \frac{k_S}{2} \langle \delta \psi^l | P_S | \delta \psi^l \rangle_{\mathbb{C}^n} \right] dt. \quad (25)$$

Substituting (16) in (24) and using (4) we arrive at

$$\begin{aligned} & \mathcal{J}(\mathbf{u} + \delta \mathbf{u}) - \mathcal{J}(\mathbf{u}) - R \\ &= \frac{\gamma \mu_B g}{3 \cdot 2^{p-1}} \sum_{l=1}^{3 \cdot 2^p} \sum_{i=x,y,z} \int_0^T \int_t^T \operatorname{Im} \langle \chi^l(\tau) | S_{1i} + S_{2i} | \psi^l(\tau) \rangle_{\mathbb{C}^n} e^{\gamma(t-\tau)} \delta u_i(t) d\tau dt \\ &= \left\langle \frac{\gamma \mu_B g}{3 \cdot 2^{p-1}} \sum_{l=1}^{3 \cdot 2^p} \int_t^T \operatorname{Im} \langle \chi^l(\tau; \mathbf{u}) | S_1 + S_2 | \psi^l(\tau; \mathbf{u}) \rangle_{\mathbb{C}^n} e^{\gamma(t-\tau)} d\tau, \delta \mathbf{u} \right\rangle_{L_2^3(0,T;\mathbb{R}^3)} \end{aligned} \quad (26)$$

which implies (10), provided that

$$R = o(\|\delta \mathbf{u}\|_{L_2^3(0,T;\mathbb{R}^3)}) \quad \text{as } \|\delta \mathbf{u}\|_{L_2^3(0,T;\mathbb{R}^3)} \rightarrow 0. \quad (27)$$

From (17),(20),(21) it follows that

$$|R| \leq C_3 [\|\delta \psi\|_{C(0,T;\mathbb{C}^n)}^2 + \|\delta \mathbf{v}\|_{L_1^3(0,T;\mathbb{R}^3)} \|\delta \psi\|_{C(0,T;\mathbb{C}^k)}] \leq C_4 \|\delta \mathbf{u}\|_{L_1^3(0,T;\mathbb{R}^3)}^2.$$

By applying Cauchy-Bunyakowski-Schwarz (CBS) inequality we deduce the estimation

$$|R| \leq C_4 T \|\delta \mathbf{u}\|_{L_2^3(0,T;\mathbb{R}^3)}^2. \quad (28)$$

From (26), (28) we deduce that

$$\delta \mathcal{J}(\mathbf{u}) = \left\langle \frac{\partial \mathcal{H}}{\partial \mathbf{u}}, \delta \mathbf{u} \right\rangle_{L_2^3(0,T;\mathbb{R}^3)} + o(\|\delta \mathbf{u}\|_{L_2^3(0,T;\mathbb{R}^3)}), \quad \text{as } \|\delta \mathbf{u}\|_{L_2^3} \rightarrow 0, \quad (29)$$

which proves the Fréchet differentiability and the formula for the gradient. \square

The Fréchet differentiability results in Theorem 1 implies the following necessary condition for the optimality.

Corollary 1 *Let $\mathbf{u}^* \in \mathcal{V}$ be an optimal value of \mathcal{J} . Then, for every $\mathbf{u} \in \mathcal{V}$ we have*

$$\sum_{l=1}^{3 \cdot 2^p} \left\langle \int_t^T \operatorname{Im} \langle \chi^l(\tau; \mathbf{u}^*) | S_1 + S_2 | \psi^l(\tau; \mathbf{u}^*) \rangle_{\mathbb{C}^n} e^{\gamma(t-\tau)} d\tau, \mathbf{u}^* - \mathbf{u} \right\rangle_{L_2^3(0,T;\mathbb{R}^3)} \geq 0. \quad (30)$$

V. PONTRYAGIN MAXIMUM PRINCIPLE

The optimality condition (30) is equivalent to the following integral form of the Pontryagin Maximum Principle:

Corollary 2 (integral form of Pontryagin Maximum Principle) *Let $\mathbf{u}^* \in \mathcal{V}$ be an optimal control. Then,*

$$\max_{\mathbf{u} \in \mathcal{V}} \int_0^T \mathcal{H}(\psi(t; \mathbf{u}^*), \mathbf{u}, \chi(t; \mathbf{u}^*)) dt = \int_0^T \mathcal{H}(\psi(t; \mathbf{u}^*), \mathbf{u}^*(t), \chi(t; \mathbf{u}^*)) dt \quad (31)$$

Next, we formulate the *Pontryagin Maximum Principle*:

Theorem 2 (Pontryagin Maximum Principle) *Let $\mathbf{u}^* \in \mathcal{V}$ be an optimal control. Then, for almost every $t \in [0, T]$, we have*

$$\max_{\mathbf{u} \in V} \mathcal{H}(\psi(t; \mathbf{u}^*), \mathbf{u}, \chi(t; \mathbf{u}^*)) = \mathcal{H}(\psi(t; \mathbf{u}^*), \mathbf{u}^*(t), \chi(t; \mathbf{u}^*)). \quad (32)$$

Proof. Let $\mathbf{u}^* \in \mathcal{V}$ be an optimal control, and $\delta \mathbf{u} \in L_2^3(0, T; \mathbb{R}^3)$ be an admissible control variation, i.e. $\mathbf{u}^* + \delta \mathbf{u} \in \mathcal{V}$. We have

$$\delta \mathcal{J}(\mathbf{u}^*) = \mathcal{J}(\mathbf{u}^* + \delta \mathbf{u}) - \mathcal{J}(\mathbf{u}^*) \leq 0. \quad (33)$$

Let $t \in (0, T)$ be a Lebesgue point for the optimal control \mathbf{u}^* . For any fixed vector $\mathbf{v} \in V$, and for all sufficiently small $\epsilon > 0$, consider a special control variation

$$\delta \mathbf{u}(t) = \begin{cases} \mathbf{v} - \mathbf{u}^*(\tau), & t - \epsilon \leq \tau \leq t + \epsilon, \\ 0, & \tau \in [0, T] \setminus [t - \epsilon, t + \epsilon]. \end{cases} \quad (34)$$

From (26) it follows that

$$\begin{aligned} \delta \mathcal{J}(\mathbf{u}^*) &= \int_{t-\epsilon}^{t+\epsilon} \left[\mathcal{H}(\psi(\tau; \mathbf{u}^*), \mathbf{v}, \chi(\tau; \mathbf{u}^*)) \right. \\ &\quad \left. - \mathcal{H}(\psi(\tau; \mathbf{u}^*), \mathbf{u}^*(\tau), \chi(\tau; \mathbf{u}^*)) \right] d\tau + R. \end{aligned} \quad (35)$$

Since vector functions $\psi(\cdot; \mathbf{u}^*)$ and $\chi(\cdot; \mathbf{u}^*)$ are continuous on $[0, T]$, t is a Lebesgue point of the integrand in (35). Therefore, we have

$$\begin{aligned} \lim_{\epsilon \rightarrow 0} \frac{1}{2\epsilon} \int_{t-\epsilon}^{t+\epsilon} \left[\mathcal{H}(\psi(\tau; \mathbf{u}^*), \mathbf{v}, \chi(\tau; \mathbf{u}^*)) - \mathcal{H}(\psi(\tau; \mathbf{u}^*), \mathbf{u}^*(\tau), \chi(\tau; \mathbf{u}^*)) \right] d\tau = \\ \mathcal{H}(\psi(t; \mathbf{u}^*), \mathbf{v}, \chi(t; \mathbf{u}^*)) - \mathcal{H}(\psi(t; \mathbf{u}^*), \mathbf{u}^*(t), \chi(t; \mathbf{u}^*)). \end{aligned} \quad (36)$$

By applying CBS inequality, from (28) we deduce that

$$\frac{1}{2\epsilon}R \leq C_4 \|\delta \mathbf{u}\|_{L^3_2(t-\epsilon, t+\epsilon; \mathbb{R}^3)}^2 \rightarrow 0, \quad \text{as } \epsilon \rightarrow 0. \quad (37)$$

Dividing (35) by 2ϵ , passing to the limit as $\epsilon \rightarrow 0$, and using (33), (36) and (37) it follows that

$$\mathcal{H}(\psi(t; \mathbf{u}^*), \mathbf{v}, \chi(t; \mathbf{u}^*)) \leq \mathcal{H}(\psi(t; \mathbf{u}^*), \mathbf{u}^*(t), \chi(t; \mathbf{u}^*)). \quad (38)$$

Since $\mathbf{v} \in V$ is arbitrary, and Lebesgue points of \mathbf{u}^* are dense in $[0, T]$, *Pontryagin maximum principle* (32) follows. \square

From PMP (32) it follows that the optimal control is of *bang-bang* type, meaning that each component switches between lower and upper bounds of prism V . Precisely, it follows from Theorem 2 that if $\mathbf{u}^* \in \mathcal{V}$ is an optimal control, then

$$u_i^* = \begin{cases} M_i, & \text{if } \text{sign} \sum_{l=1}^{3 \cdot 2^p} \int_t^T \text{Im} \langle \chi^l(\tau) | S_{1i} + S_{2i} | \psi^l(\tau) \rangle_{\mathbb{C}^n} e^{\gamma(t-\tau)} d\tau > 0; \\ m_i, & \text{if } \text{sign} \sum_{l=1}^{3 \cdot 2^p} \int_t^T \text{Im} \langle \chi^l(\tau) | S_{1i} + S_{2i} | \psi^l(\tau) \rangle_{\mathbb{C}^n} e^{\gamma(t-\tau)} d\tau < 0, \end{cases} \quad (39)$$

for $i = x, y, z$, where $\psi = \psi(\cdot; \mathbf{u}^*)$ and $\chi = \chi(\cdot; \mathbf{u}^*)$ are the corresponding optimal states. Hence, the formula (39) expresses optimal control \mathbf{u}_* in terms of optimal states $\psi = \psi(\cdot; \mathbf{u}^*)$ and $\chi = \chi(\cdot; \mathbf{u}^*)$:

$$\mathbf{u}^* = \Gamma(\psi, \chi), \quad (40)$$

where $\Gamma = (\Gamma_i, i = x, y, z)$ be a vector-function with components

$$\Gamma_i(\psi, \chi) = \frac{M_i - m_i}{2} \text{sign} \sum_{l=1}^{3 \cdot 2^p} \int_t^T \text{Im} \langle \chi^l(\tau) | S_{1i} + S_{2i} | \psi^l(\tau) \rangle_{\mathbb{C}^n} e^{\gamma(t-\tau)} dt + \frac{M_i + m_i}{2}, \quad i = x, y, z. \quad (41)$$

Γ is an *optimal control synthesizing function*. Using expression (6), one express the corresponding optimal magnetic field in terms of the optimal states $\psi = \psi(\cdot; \mathbf{u}^*)$ and $\chi = \chi(\cdot; \mathbf{u}^*)$:

$$\mathbf{v}(\cdot; \mathbf{u}^*) = \mathbf{v}(\cdot; \Gamma(\psi, \chi)). \quad (42)$$

By substituting (42) in (1) and (11) we deduce that the optimal states ψ and χ must satisfy the following nonlinear closed-loop system of $3 \cdot 2^{2(p+1)}$ integro-differential equations with

two-end boundary values:

$$i\hbar \frac{d\psi^l}{dt} = \mathbf{H}(\mathbf{v}(t; \Gamma(\psi, \chi))), \quad \text{in } (0, T]; \quad \psi^l(0) = \psi_T^l \in \mathbb{C}^n; \quad (43)$$

$$i\hbar \frac{d\chi^l}{dt} = \mathbf{H}^*(\mathbf{v}(t; \Gamma(\psi, \chi))) - i\frac{k_S}{2}P_S\psi^l, \quad \text{in } (0, T]; \quad \chi^l(T) = 0 \in \mathbb{C}^n, \quad (44)$$

for $l = 1, \dots, 3 \cdot 2^p$.

Hence, *Pontryagin Maximum Principle* implies the following explicit two-step method (EPMP) for the identification of the optimal electromagnetic field input:

Step 1.: Solve the nonlinear closed system of integro-differential equations (43),(44) to find optimal state and adjoined vector-functions

$$(\psi, \chi) : [0, T] \rightarrow \mathbb{C}^{3 \cdot 2^{2(p+1)}} \times \mathbb{C}^{3 \cdot 2^{2(p+1)}};$$

Step 2.: Use *optimal control synthesizing function* Γ to find a bang-bang optimal control \mathbf{u}^* from (40), and continuous in-time optimal electromagnetic field input \mathbf{v}^* from (42).

EPMP method is computationally expensive. In the next section we suggest an iterative method based on the PMP.

Remark. It is essential to note that our model assumes that the radical pair system is a pure system described by the Schrödinger system, and doesn't take into account many factors, including the interaction with the environment [35], decoherence and spin relaxation phenomena [52–57]. Therefore, the natural question is what is the limitation of the characterization of the *quantum coherence* through *Pontryagin Maximum Principle* in terms of system complexity? Remarkably, applicability of the Pontryagin Maximum Principle and characterization of the quantum coherence via bang-bang optimal control is relevant for a broad class of quantum optimal control framework. Mathematically, it is hidden in the bilinear structure of the Hamilton-Pontryagin function with respect to state and control variables. In particular, replacing the phenomenological reaction term \mathbf{K} in (5) via the fundamental quantum dynamical evolution of radical pair recombination reaction term derived from the quantum measurement theory and incorporating quantum Zeno effect [52] would preserve relevance of the Pontryagin Maximum Principle for the characterization of the quantum coherence and bang-bang structure of the optimal control.

VI. ALGORITHMS

A. Gradient Projective Method (GPM) in Hilbert Space

Fréchet differentiability result Theorem 1 implies the following gradient method in the Hilbert space $L_2^3(0, T; \mathbb{R}^3)$.

Step 1. Set $N = 0$ and define initial control $\mathbf{u}^0 \in \mathcal{V}$.

Step 2. Compute magnetic field $\mathbf{v}^N = \mathbf{v}^N(\cdot; \mathbf{u}^N)$ using filter expression (6) for given $\mathbf{v}_0 \in \mathbb{R}^3$ and filter parameter $\gamma > 0$.

Step 3. Solve Schrödinger equation (1) using \mathbf{v}^N to find $\psi^N = \psi(\cdot; \mathbf{u}^N)$ and compute corresponding cost $\mathcal{J}(\mathbf{u}^N)$.

Step 4. If $N = 0$, move to the next step. Otherwise, check the following criteria

$$\left| \frac{\mathcal{J}(\mathbf{u}^N) - \mathcal{J}(\mathbf{u}^{N-1})}{\mathcal{J}(\mathbf{u}^N)} \right| < \epsilon_1 \quad \text{and} \quad \frac{\|\mathbf{u}^N - \mathbf{u}^{N-1}\|_{L_2^3(0, T; \mathbb{R}^3)}}{\|\mathbf{u}^N\|_{L_2^3(0, T; \mathbb{R}^3)}} < \epsilon_2, \quad (45)$$

where $\epsilon_1, \epsilon_2 > 0$ are required tolerance errors. If (45) is verified, then terminate the iteration process. Otherwise, move to the next step.

Step 5. Use ψ^N and v^N to solve the adjoint problem (11) in order to find $\chi^N = \chi^N(\cdot; u^N)$ and compute gradient $\mathcal{J}'(\mathbf{u}^N)$ using expression (10).

Step 6. Choose step-size parameter $\lambda_N > 0$ and compute new control \mathbf{u}^{N+1} as follows

$$\mathbf{u}^{N+1} = \mathbf{u}^N + \lambda_N \cdot \mathcal{J}'(\mathbf{u}^N). \quad (46)$$

Step 7. Replace $\mathbf{u}^{N+1} = \text{proj}_V(\mathbf{u}^{N+1})$, where

$$\text{proj}_V(\mathbf{u}^{N+1}) := \begin{cases} m_i, & \text{if } \mathbf{u}_i^{N+1} \leq m_i; \\ u_i^{N+1}, & \text{if } m_i < \mathbf{u}_i^{N+1} < M_i; \text{ for } i = x, y, z. \\ M_i, & \text{if } u_i^{N+1} \geq M_i; \end{cases} \quad (47)$$

Then, replace N with $N + 1$ and move to Step 2.

Remark. The learning rate λ_N in Step 6 is calculated for each iteration and based on the Barzilai-Borwein method. Indeed, we compute λ_N proportional to λ_{BB}^N , where

$$\lambda_{BB}^N = \left| \frac{\langle \mathbf{u}^N - \mathbf{u}^{N-1}, \mathcal{J}'(\mathbf{u}^N) - \mathcal{J}'(\mathbf{u}^{N-1}) \rangle_{L_2^3(0, T; \mathbb{R}^3)}}{\|\mathcal{J}'(\mathbf{u}^N) - \mathcal{J}'(\mathbf{u}^{N-1})\|_{L_2^3(0, T; \mathbb{R}^3)}} \right|. \quad (48)$$

B. Iterative Pontryagin Maximum Principle (IPMP) Method

Pontryagin Maximum Principle and two-step EPMP method suggests the following iterative algorithm to solve the optimal control problem.

Step 1. Set $N = 0$ and define initial control $\mathbf{u}^0 \in \mathcal{V}$.

Step 2. Compute magnetic field $\mathbf{v}^N = \mathbf{v}^N(\cdot; \mathbf{u}^N)$ using filter expression (6) for given $\mathbf{v}_0 \in \mathbb{R}^3$ and filter parameter $\gamma > 0$.

Step 3. Solve Schrödinger system (1) and its adjoint (11) using \mathbf{v}^N to find $\psi^N = \psi(\cdot; \mathbf{u}^N)$ and $\chi^N = \chi^N(\cdot; \mathbf{u}^N)$, respectively.

Step 4. Compute a new control vector by using (40)

$$\mathbf{u}^{N+1} = \Gamma(\psi^N, \chi^N), \quad (49)$$

i.e.

$$u_i^{N+1} = \begin{cases} M_i, & \text{if } \Gamma_i(\psi(\cdot; \mathbf{u}^N), \chi(\cdot; \mathbf{u}^N)) > 0; \\ m_i, & \text{if } \Gamma_i(\psi(\cdot; \mathbf{u}^N), \chi(\cdot; \mathbf{u}^N)) < 0, \quad i = x, y, z. \end{cases} \quad (50)$$

Step 5. If $\mathbf{u}^{N+1} = \mathbf{u}^N$, terminate the iteration process. Otherwise, replace N with $N + 1$ and move to Step 2.

Note that IPMP algorithm at every iteration solves linear Schrödinger system (1) and its adjoint (11), and produces a new bang-bang control vector by (49). Whenever $\mathbf{u}^{N+1} = \mathbf{u}^N$ is fulfilled, then \mathbf{u}^N satisfy PMP relation (40), (41), and therefore is a candidate to be a bang-bang optimal control, and accordingly $\mathbf{v}^N = \mathbf{v}(\cdot; \mathbf{u}^N)$ is a candidate to be a continuous in-time optimal electromagnetic field input.

VII. NUMERICAL RESULTS

This section presents numerical results obtained by implementing the algorithms described in Section VI. Here, we considered the dynamics for the model as described in Section II for $p = 1, \dots, 7$ proton cases with spin-1/2 and time length $T = 0.5\mu s$. Constant rates for the decay are chosen as $k_S = k_T = 10\hbar$. Constant-in-time hyperfine $A = (A_j)_{j=1, \dots, p}$

is set as follows:

$$\begin{aligned} A_1 &= [-0.234, -0.234, 0.117]; \\ A_2 &= [-0.030, -0.022, 0.688]; \\ A_3 &= [0.238, 0.357, 0.117]; \\ A_j &= [-0.218, -0.202, -0.054], \quad \text{for } j = 4, \dots, p, \end{aligned}$$

all in millitesla (mT).

A 200 points discretization of the time interval $[0, T]$ was considered, and solutions of the Schrödinger system (1) and its adjoint (11) were obtained using an adaptation of 4th order Runge-Kutta method.

Remark. No-filter model was considered in [32], where adapted algorithms were derived and implemented. Yield values of approximated optimal controls for the no-filter case mentioned in this section were considered and calculated according to the results of [32].

A. Prism Case 1.

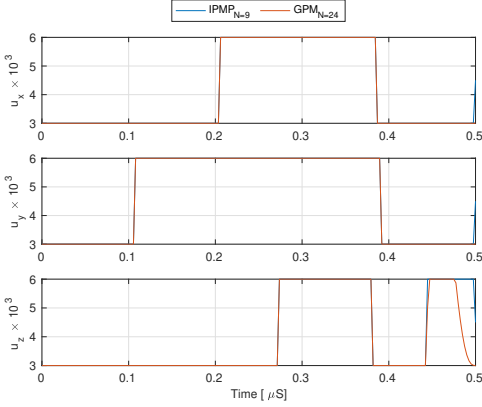
In this subsection, we choose a prism V_1 with positive bounds $m_i = 3\mu\text{T}$ and $M_i = 6\mu\text{T}$ and consider a control set

$$\mathcal{V}_1 := \left\{ \mathbf{u} \in L_2^3(0, T; \mathbb{R}^3) : \mathbf{u}(t) \in V_1 = \prod_{i=x,y,z} [3, 6], \text{ a.e. } t \in [0, T] \right\}.$$

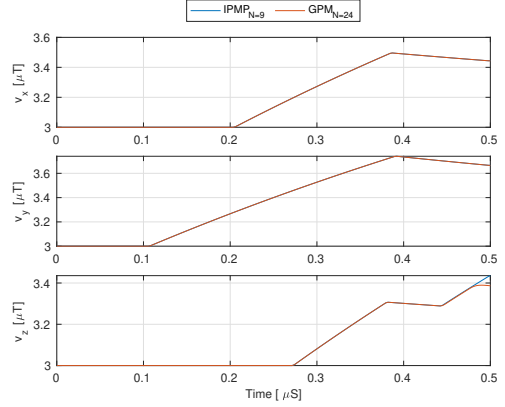
Next, we demonstrate the numerical results based on GPM and IPMP algorithms for m-proton model cases with $m \leq 7$. Our numerical analysis focus on the convergence of both methods to unique optimal solution, robustness of the methods with respect to selection of the initial iteration, comparison with no-filter model, effect of the free filtering parameters $\gamma > 0$ and $\mathbf{v} \in \mathbb{R}^3$.

1 Proton Case. We start by comparing the approximate solutions of IPMP and GPM. Filtering parameters are set to $\mathbf{v}_0 = [3, 3, 3]\mu\text{T}$ and $\gamma = 1$. Figure 1 shows the calculated optimal control (left) and magnetic field (right) for both IPMP and GPM algorithms with initial constant-in-time control vector being selected as $\mathbf{u}^0(t) = [3, 3, 3]\mu\text{T}$. The GPM so-

lution was obtained after 24 iterations, whereas the IPMP method converged only in 9 iterations.



(a) Control coordinates obtained for the IPMP (blue) and GPM (red) methods at the last iteration.



(b) Magnetic field coordinates obtained for the IPMP (blue) and the GPM (red) methods at the last iteration.

FIG. 1: Approximated optimal control and magnetic field obtained for the 1-proton case and initial control $\mathbf{u}^0(t) = [3, 3, 3]\mu T$. Filtering parameters are $\mathbf{v}_0 = [3, 3, 3]\mu T$ and $\gamma = 1$. # of iterations were 24 for GPM and 9 for IPMP algorithms.

Next, we compare the results with the no-filter case. Figure 2 demonstrates the dependence of the scaled maximum value of the cost functional \mathcal{J} on a sample of increasing filter parameter values γ ; here, we set $\mathbf{u}^0(t) = [3, 3, 3]\mu T$ and use the IPMP algorithm only. Dashed line in Figure 2 corresponds to the scaled maximum value of the cost functional in the no-filter model, i.e. the scaled maximum value of the quantum singlet yield. Colored graphs correspond to various filtered cases with different choices of the free filtering parameter \mathbf{v} . First, we observe that by increasing the value of the filtering parameter γ , the maximum of the cost functional asymptotically approaches the maximum value in the no-filter case. To assess the effect of filtering, it is essential to note all the graphs for the filtered cases are below the dashed line, meaning that the trading off between the original non-filtered model with bang-bang optimal magnetic field and filtered model with continuous in time optimal magnetic field is associated with some loss of the maximum singlet yield expressed as a maximum of the cost functional. In Table 1 we collected the minimum and maximum yield loss by applying filtering with all selected values of parameters γ and

\mathbf{v} shown in Figure 2, and with various selection of initial iteration \mathbf{u}_0 . Remarkably, in all cases loss of the quantum singlet yield is less than 1%. This is the very strong argument on behalf of the filtered model with the gain of regularity of the optimal electromagnetic field input. Numerical results in Figure 2 also demonstrate the role and importance of the selection of the filtering parameter \mathbf{v}_0 : minimal yield loss is achieved if the initial value \mathbf{v}_0 of the magnetic field in all filtered cases is selected as a value of the bang-bang optimal magnetic field at initial moment $t = 0$ in non-filtered model.

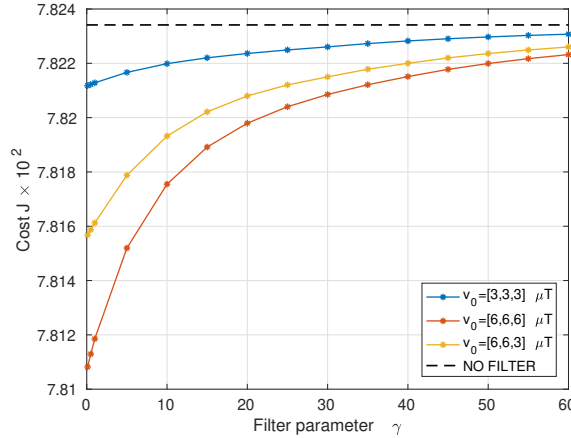
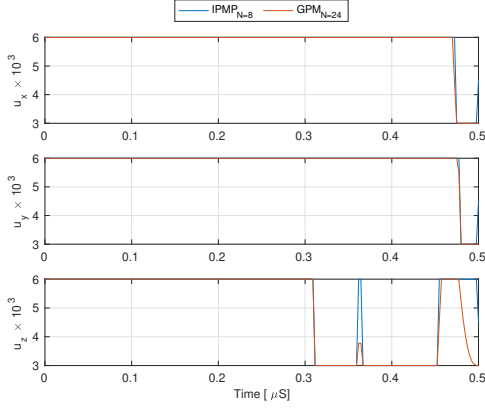


FIG. 2: 1-proton case. Asymptotic of \mathcal{J} for a sample of increasing values of γ . The dashed line corresponds to the cost value of the approximated optimal control for the no-filter model. Minimum and maximum yield loss (in %) for each case of \mathbf{v}_0 is shown in Table I.

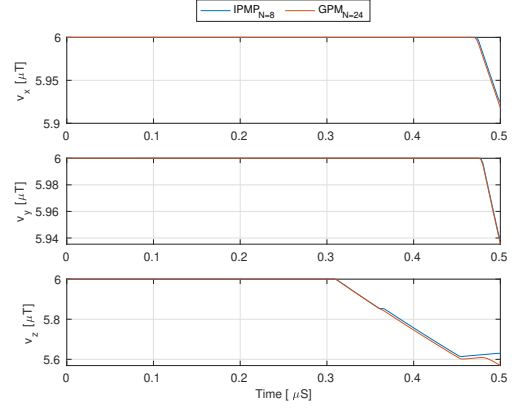
2-7 Proton Cases. All the main conclusions outlined in 1 Proton Case are confirmed in 2-7 Proton Cases. The results are presented in Figures 3-14 and Table I.

The following are the main outcomes of numerical simulations of up to 7-proton models with positive range of the control parameter:

- Both IPMP and GPM methods converges to the unique bang-bang optimal control and produce the same unique continuous in time optimal electromagnetic field input. The simulations show that IPMP provides an approximated optimal control within 5-10 iterations, whereas GPM approximated solutions require at least 2 times more iterations. This advantage of IPMP over the GPM method is even more apparent for higher proton models when computational cost increases exponentially.
- Numerical simulations of up to 7-proton models with filtering parameter range $0.1 \leq$



(a) Control coordinates obtained for the IPMP (blue) and GPM (red) methods at the last iteration.



(b) Magnetic field coordinates obtained for the IPMP (blue) and the GPM (red) methods at the last iteration.

FIG. 3: Approximated optimal control and magnetic field obtained for the 2-proton case and initial control $\mathbf{u}^0(t) = [3, 3, 3]\mu T$. Filtering parameters are $\mathbf{v}_0 = [6, 6, 6]\mu T$ and $\gamma = 1$. # of iterations were 24 for GPM and 8 for IPMP algorithms.

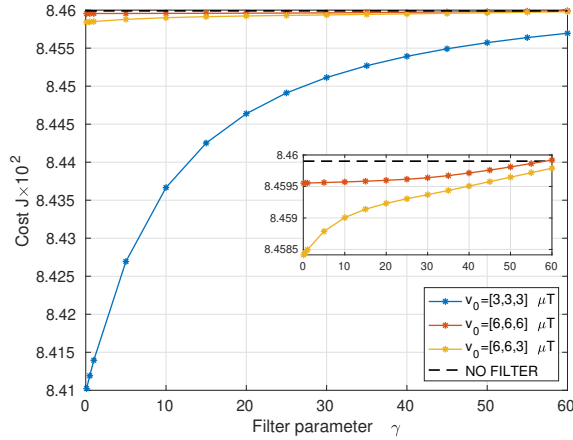
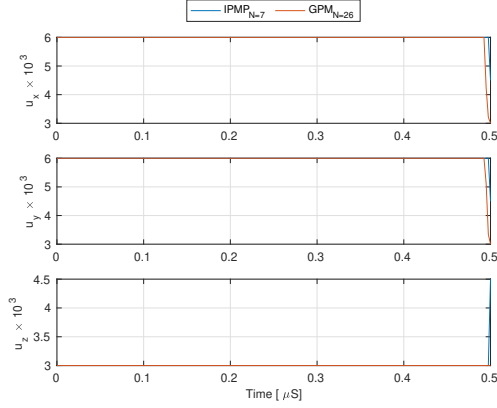


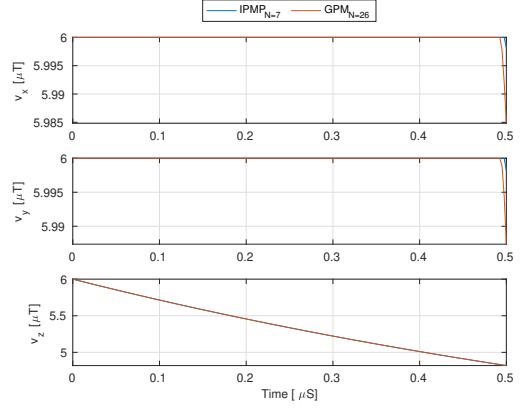
FIG. 4: 2-proton. Asymptotic of \mathcal{J} for a sample of increasing values of γ . The dashed line corresponds to the cost value of the approximated optimal control for the no-filter model.

Minimum and maximum yield loss (in %) for each case of \mathbf{v}_0 is shown in Table I.

$\gamma \leq 60$, and with various selection of initial iterations demonstrate that trading off between the original non-filtered model with bang-bang optimal magnetic field and filtered model with continuous in time optimal magnetic field is associated with the loss of the maximum singlet yield expressed as a maximum of the cost functional within



(a) Control coordinates obtained for the IPMP (blue) and GPM (red) methods at the last iteration.



(b) Magnetic field coordinates obtained for the IPMP (blue) and the GPM (red) methods at the last iteration.

FIG. 5: Approximated optimal control and magnetic field obtained for the 3-proton case and initial control $\mathbf{u}^0(t) = [3, 3, 3]\mu T$ and filtering parameters are $\mathbf{v}_0 = [6, 6, 6]\mu T$ and $\gamma = 1$. # of iterations were 26 for GPM and 7 for IPMP algorithms.

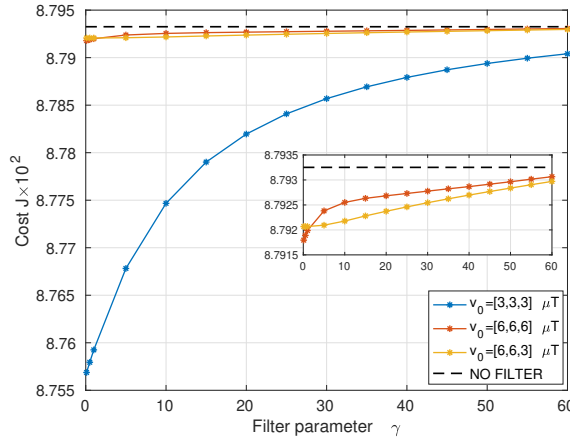
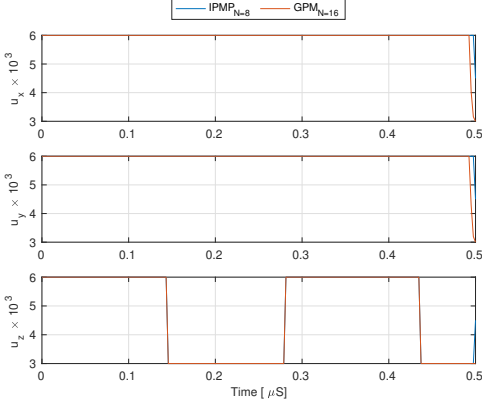


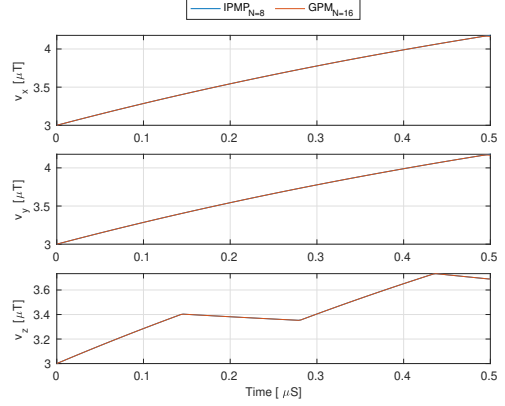
FIG. 6: 3-proton. Asymptotic of \mathcal{J} for a sample of increasing values of γ . The dashed line corresponds to the cost value of the approximated optimal control for the no-filter model.

Minimum and maximum yield loss (in %) for each case of \mathbf{v}_0 is shown in Table I.

1%. Hence, filtering presents a powerful regularization tool to replace optimal bang-bang electromagnetic field input with the continuous in time electromagnetic field wave which produces almost the same quantum singlet yield, and possibly preserves the quantum coherence of the radical pair system.



(a) Control coordinates obtained for the IPMP (blue) and GPM (red) methods at the last iteration.



(b) Magnetic field coordinates obtained for the IPMP (blue) and the GPM (red) methods at the last iteration.

FIG. 7: Approximated optimal control and magnetic field obtained for the 4-proton case and initial control $u^0 = 3\mu T$. Filtering parameters are $\mathbf{v}_0 = 6\mu T$ and $\gamma = 1$. # of iterations were 16 for GPM and 5 for IPMP algorithms.

- Numerical simulations demonstrate that the best selection of filtering parameters γ and \mathbf{v}_0 in terms of minimal loss of quantum singlet yield is achieved by choosing γ large, and by selecting initial value of the magnetic field \mathbf{v}_0 to match the initial value of the optimal bang-bang magnetic field in no-filter model.

B. Prism Case 2.

To assess the effect of control parameter with sign changing range, in this subsection, we choose a prism V_1 with bounds $m_i = 3\mu T$, $M_i = 6\mu T$, $i = x, y$, $m_z = -1\mu T$ and $M_z = 2\mu T$ and consider a control set

$$\mathcal{V}_2 = \left\{ \mathbf{u} \in L_2^3(0, T; \mathbb{R}^3) : \mathbf{u}(t) \in V_2 = [3, 6]^2 \times [-1, 2], \text{ a.e. } t \in [0, T] \right\}.$$

In [32] (section 7.3) it is demonstrated that in case of control parameter range chosen as V_2 there is a non-uniqueness of the optimal control, and the numerical methods based on PMP algorithm present only local convergence and stability. Here our goal is to analyze the effect of filtering on the phenomena of non-uniqueness of the optimal control.

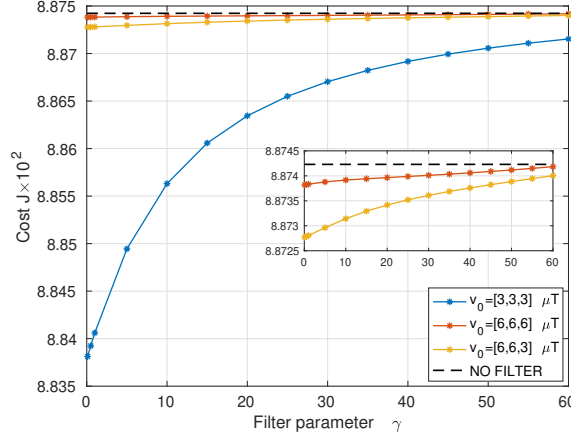


FIG. 8: 4-proton. Asymptotics of the cost functional \mathcal{J} for a sample of increasing filter parameter values γ . The dashed line corresponds to the cost value of the approximated optimal control for the no-filter (NF) model. Minimum and maximum yield loss (in %) for each case of v_0 is shown in Table I.

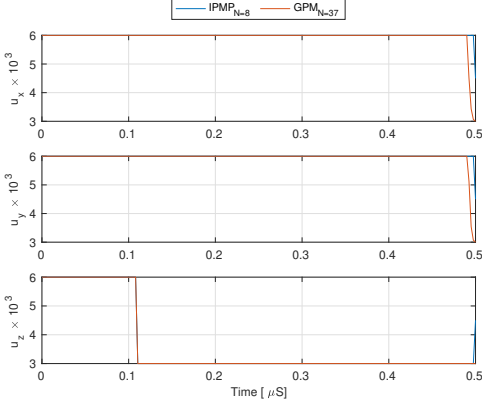
TABLE I: Minimum and Maximum yield loss (in %), concerning γ , relative to the yield of the corresponding approximated optimal control for the no-filter model, for different initial controls u_0 and each case of number of protons.

\mathbf{u}_0	[3, 3, 3] μT		[6, 6, 6] μT		[6, 6, 3] μT	
Proton Case	min	max	min	max	min	max
1	0.0043	0.0286	0.0139	0.1610	0.0104	0.0989
2	0.0348	0.5872	-0.0002	0.0041	0.0013	0.0176
3	0.0323	0.4137	0.0021	0.0166	0.0032	0.0135
4	0.0304	0.4069	0.0005	0.0046	0.0025	0.0164
5	0.0281	0.3775	-0.0008	0.0041	0.0014	0.0152
6	0.0282	0.3659	-0.0004	0.0030	0.0022	0.0184
7	0.0274	0.3486	-0.0008	0.0026	0.0163	0.0190

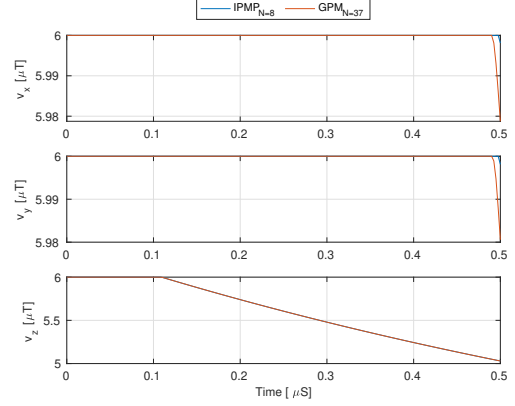
Let us consider the following two grids with 27 points in each built around the vertices $(6, 6, -1)$ and $(6, 6, 2)$ respectively.

$$u_{ijk}^1 = [6, 6, -1] + 0.5 \cdot [1 - i, 1 - j, 1 - k];$$

$$u_{ijk}^2 = [6, 6, 2] + 0.5 \cdot [1 - i, 1 - j, 1 - k];$$



(a) Control coordinates obtained for the IPMP (blue) and GPM (red) methods at the last iteration.



(b) Magnetic field coordinates obtained for the IPMP (blue) and the GPM (red) methods at the last iteration.

FIG. 9: Approximated optimal control and magnetic field obtained for the 5-proton case and initial control $\mathbf{u}^0(t) = [6, 6, 6]\mu T$. Filtering parameters are $\mathbf{v}_0 = [6, 6, 6]\mu T$ and $\gamma = 1$. # of iterations were 37 for GPM and 8 for IPMP algorithms.

for $i, j, k = 0, 1, 2$. In [32] it is demonstrated that choosing initial control parameters from two different grids imply the convergence to two different bang-bang optimal controls in a 1-proton model. Next, we demonstrate the numerical results with IPMP algorithm, and analyze the effect of free filtering parameters $\gamma > 0$ and $\mathbf{v} \in \mathbb{R}^3$ on non-uniqueness of the optimal control.

1 Proton Case. We choose a filter parameter $\gamma = 1$. Applying the IPMP algorithm, we calculate optimal bang-bang control \mathbf{u}_{ijk} (respectively $\tilde{\mathbf{u}}_{ijk}$) with initial iteration chosen as a constant in-time control vector equal to grid points \mathbf{u}_{ijk}^1 (respectively \mathbf{u}_{ijk}^2). Figure 15 (respectively Figure 16) shows the coordinates of optimal controls \mathbf{u}_{ijk} (respectively $\tilde{\mathbf{u}}_{ijk}$) for each case of the initial magnetic field $\mathbf{v}_0 = [6, 6, -1]\mu T$ and $\mathbf{v}_0 = [6, 6, 2]\mu T$.

Then, with computer accuracy we have

$$\max_{\mathbf{u}^1 \in \{\mathbf{u}_{ijk}\}, \mathbf{u}^2 \in \{\tilde{\mathbf{u}}_{ijk}\}} \frac{\|\mathbf{u}^1 - \mathbf{u}^2\|_{L_2^3(0, T; \mathbb{R}^3)}}{\|\mathbf{u}^1\|_{L_2^3(0, T; \mathbb{R}^3)}} = 0,$$

$$\max_{\mathbf{u}^1 \in \{\mathbf{u}_{ijk}\}, \mathbf{u}^2 \in \{\tilde{\mathbf{u}}_{ijk}\}} \left| \frac{\mathcal{J}(\mathbf{u}^1) - \mathcal{J}(\mathbf{u}^2)}{\mathcal{J}(\mathbf{u}^1)} \right| = 0,$$

for both cases $\mathbf{v}_0 = [6, 6, -1]\mu T$ and $\mathbf{v}_0 = [6, 6, 2]\mu T$. Hence, by fixing a filtering parameters as $\gamma = 1$, and \mathbf{v}_0 as one of the vertices $[6, 6, -1]$ or $[6, 6, 2]$ we observe a convergence

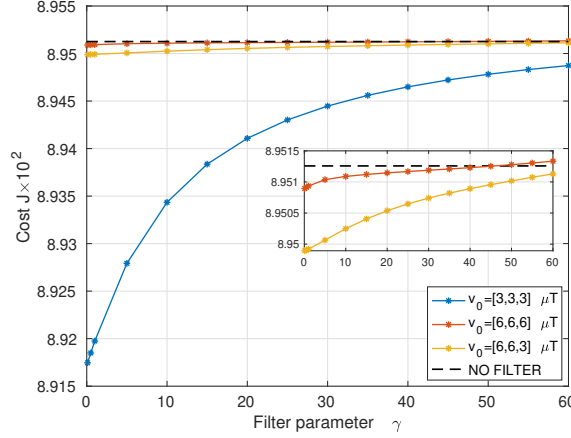


FIG. 10: 5-proton. Asymptotics of the cost functional \mathcal{J} for a sample of increasing filter parameter values γ . The dashed line corresponds to the cost value of the approximated optimal control for the no-filter (NF) case. Minimum and maximum yield loss (in %) for each case of \mathbf{v}_0 is shown in Table I.

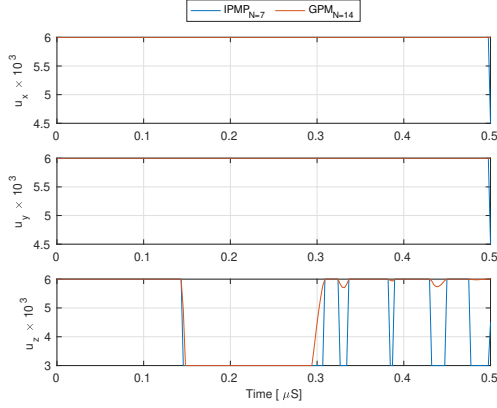
to unique bang-bang optimal control when initial iteration is selected from different grids. Next, we verify the amount of quantum singlet yield loss associated with filtering versus no-filter model. Let $\hat{\mathbf{u}}_{ijk}$ (respectively $\check{\mathbf{u}}_{ijk}$) be a bang-bang control obtained using the IPMP algorithm for the points in the grid \mathbf{u}_{ijk}^1 (respectively \mathbf{u}_{ijk}^2) selected as initial iteration in the no-filter model. Then we have

$$\max_{\mathbf{u}^1 \in \{\mathbf{u}_{ijk}^1\}, \mathbf{u}^2 \in \{\hat{\mathbf{u}}_{ijk}\}} \left| \frac{\mathcal{J}(\mathbf{u}^1) - \mathcal{J}(\mathbf{u}^2)}{\mathcal{J}(\mathbf{u}^1)} \right| \leq 8.559762 \times 10^{-4}.$$

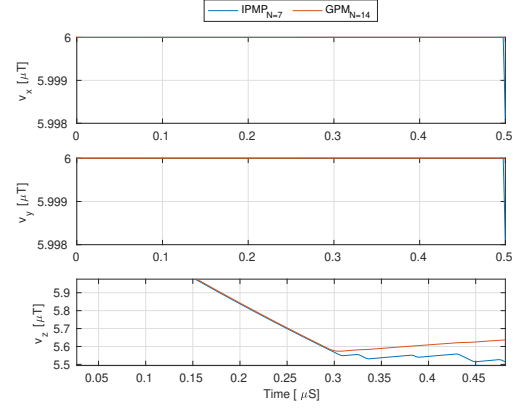
$$\max_{\mathbf{u}^1 \in \{\check{\mathbf{u}}_{ijk}\}, \mathbf{u}^2 \in \{\check{\mathbf{u}}_{ijk}\}} \left| \frac{\mathcal{J}(\mathbf{u}^1) - \mathcal{J}(\mathbf{u}^2)}{\mathcal{J}(\mathbf{u}^1)} \right| \leq 9.348020 \times 10^{-4}.$$

Hence, gaining uniqueness of the optimal control in the filtering model is associated with the loss of quantum singlet yield less than 1%.

As it is demonstrated in [32], there is a non-uniqueness of the optimal control in the original model without filtering. To demonstrate that numerically, let $\mathbf{u}^1 := \hat{\mathbf{u}}_{111}$ (respectively $\mathbf{u}^2 := \check{\mathbf{u}}_{111}$) is the bang-bang optimal control obtained by IPMP algorithm with initial iteration being a central point of the grid system $\{\mathbf{u}_{ijk}^1\}$ (respectively $\{\mathbf{u}_{ijk}^2\}$) in a no-filter model. The following discrepancy between the bang bang controls \mathbf{u}^1 and \mathbf{u}^2 , and their associated cost values demonstrate that the IPMP algorithm converges to two different bang-bang



(a) Control coordinates obtained for the IPMP (blue) and GPM (red) methods at the last iteration.



(b) Magnetic field coordinates obtained for the IPMP (blue) and the GPM (red) methods at the last iteration.

FIG. 11: Approximated optimal control and magnetic field obtained for the 6-proton case and initial control $\mathbf{u}^0(t) = [3, 3, 3]\mu T$. Filtering parameters are $\mathbf{v}_0 = [6, 6, 6]\mu T$ and $\gamma = 1$. # of iterations were 14 for GPM and 7 for IPMP algorithms.

optimal controls with approximately the same maximum value of the quantum singlet yield:

$$\left| \frac{\mathcal{J}(\mathbf{u}^1) - \mathcal{J}(\mathbf{u}^2)}{\mathcal{J}(\mathbf{u}^1)} \right| = 7.8758 \times 10^{-5};$$

$$\frac{\|\mathbf{u}^1 - \mathbf{u}^2\|_{L_2^3(0,T;\mathbb{R}^3)}}{\|\mathbf{u}^1\|_{L_2^3(0,T;\mathbb{R}^3)}} = 0.4623.$$

Next, we consider the filtered model with $\gamma = 10$ and apply the IPMP algorithm to calculate optimal bang-bang controls \mathbf{u}_{ijk} (respectively $\tilde{\mathbf{u}}_{ijk}$) for each initial data in the grid \mathbf{u}_{ijk}^1 (respectively \mathbf{u}_{ijk}^2). Numerical results demonstrate that in all cases there is no convergence to optimal control, but there is oscillations between two optimal controls. Figure 17 (respectively Figure 18) shows iterations $N = 19$ and $N = 20$ of the calculated bang-bang control \mathbf{u}_{111} (respectively $\tilde{\mathbf{u}}_{111}$) and the correspondig cost functional, for both cases $\mathbf{v}_0 = [6, 6, -1]\mu T$ and $\mathbf{v}_0 = [6, 6, 2]\mu T$. Similar behavior holds for all grid points, and the calculation of the relative cost functional discrepancy versus control parameter discrepancy for the two collection of grid points reveals the following estimates:

$$4.463655 \times 10^{-6} \leq \left| \frac{\mathcal{J}(\mathbf{u}_{ijk}^{N=20}) - \mathcal{J}(\mathbf{u}_{ijk}^{N=19})}{\mathcal{J}(\mathbf{u}_{ijk}^{N=20})} \right| \leq 7.923061 \times 10^{-6}$$

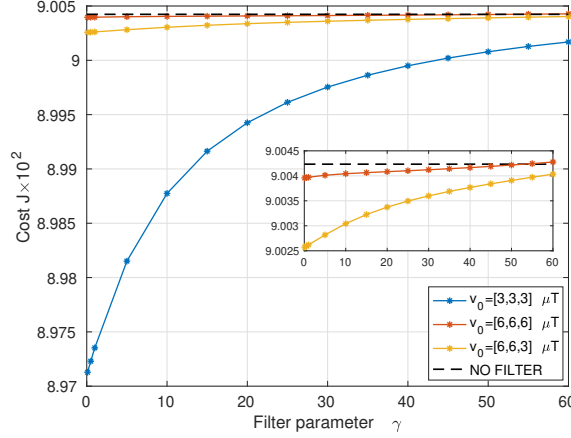


FIG. 12: 6-proton. Asymptotics of the cost functional \mathcal{J} for increasing filter parameter values γ . The dashed line corresponds to the cost value of the approximated optimal control for the no-filter (NF) model. Minimum and maximum yield loss (in %) for each case of \mathbf{v}_0 is shown in Table I.

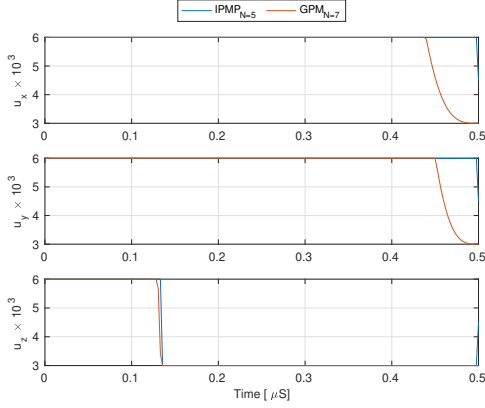
$$\begin{aligned}
3.078803 \times 10^{-1} &\leq \frac{\|\mathbf{u}_{ijk}^{N=20} - \mathbf{u}_{ijk}^{N=19}\|_{L_2^3(0,T;\mathbb{R}^3)}}{\|\mathbf{u}_{ijk}^{N=20}\|_{L_2^3(0,T;\mathbb{R}^3)}} \leq 4.364718 \times 10^{-1} \\
4.463655 \times 10^{-6} &\leq \left| \frac{\mathcal{J}(\tilde{\mathbf{u}}_{ijk}^{N=20}) - \mathcal{J}(\mathbf{u}_{ijk}^{N=19})}{\mathcal{J}(\mathbf{u}_{ijk}^{N=20})} \right| \leq 7.923123 \times 10^{-6} \\
3.085775 \times 10^{-1} &\leq \frac{\|\mathbf{u}_{ijk}^{N=20} - \mathbf{u}_{ijk}^{N=19}\|_{L_2^3(0,T;\mathbb{R}^3)}}{\|\mathbf{u}_{ijk}^{N=20}\|_{L_2^3(0,T;\mathbb{R}^3)}} \leq 4.419706 \times 10^{-1}
\end{aligned}$$

This demonstrate that the uniqueness of the optimal control fails to be true in a filtered model with $\gamma = 10$, and for every initial iteration chosen from the two different collections of grid points, the IPMP algorithm converges to two different approximate optimal control parameters.

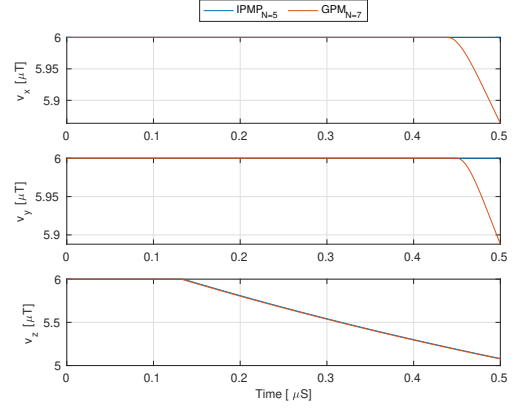
Similar behavior is observed in m -proton cases with $m \geq 2$. Hence, filtering presents a powerful regularization tool to address the non-uniqueness of the optimal control.

The following are the main outcomes of numerical simulations of m -proton model with sign changing range of the control parameter:

- In general, there is a non-uniqueness of the optimal control, and both IPMP and GPM methods demonstrate the local convergence and stability, due to non-uniqueness of the optimal control. IPMP has an advantage over GPM in terms of convergence rate and efficiency.



(a) Control coordinates obtained for the IPMP (blue) and GPM (red) methods at the last iteration.



(b) Magnetic field coordinates obtained for the IPMP (blue) and the GPM (red) methods at the last iteration.

FIG. 13: Approximated optimal control and magnetic field obtained for the 7-proton case and initial control $\mathbf{u}^0(t) = [3, 3, 3]\mu T$. Filtering parameters are $\mathbf{v}_0 = [6, 6, 6]\mu T$ and $\gamma = 1$. # of iterations were 7 for GPM and 5 for IPMP algorithms.

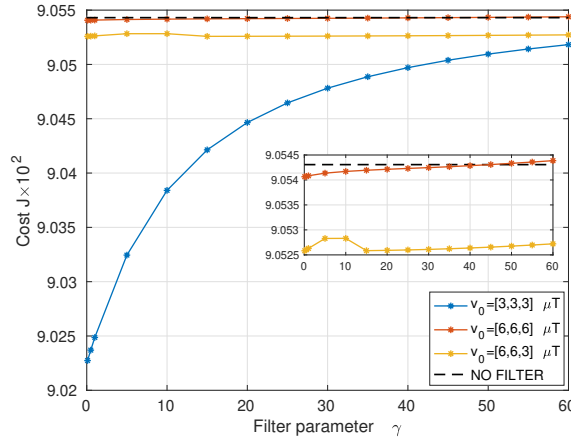
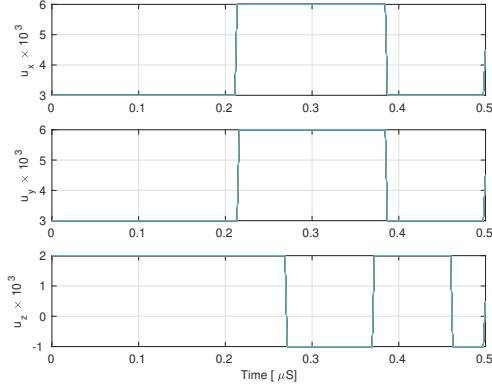
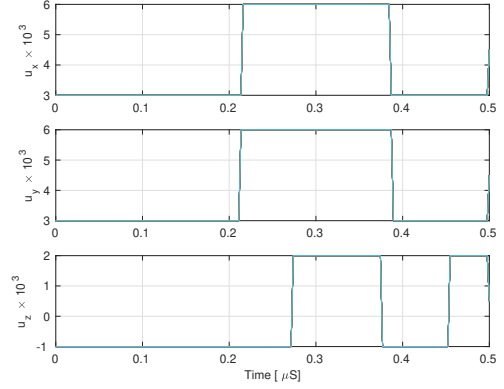


FIG. 14: 7-proton. Asymptotics of the cost functional \mathcal{J} for increasing values of γ . The dashed line corresponds to the cost of approximated optimal control for the no-filter (NF) model. Minimum and maximum yield loss (in %) for each case of v_0 is shown in Table I.

- Filtering presents a powerful regularization tool to address the non-uniqueness of the optimal control in the original no-filter model. Numerical simulations demonstrate that by choosing the filtering parameter γ small enough, the filtered optimal control problem has a unique bang-bang optimal control. Moreover, trading off between the

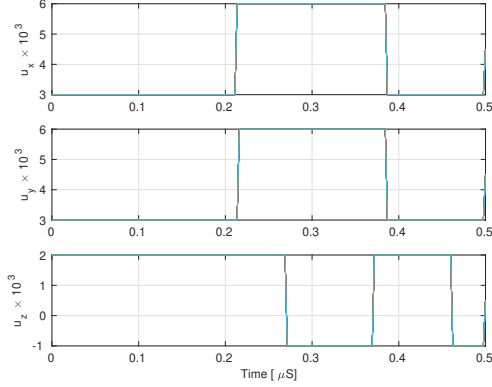


(a) Case $\mathbf{v}_0 = [6, 6, -1]\mu\text{T}$.

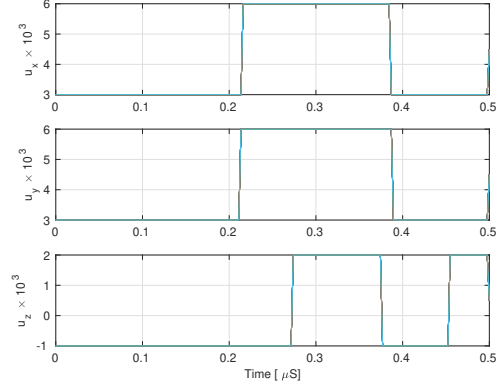


(b) Case $\mathbf{v}_0 = [6, 6, 2]\mu\text{T}$.

FIG. 15: 1-proton. Approximated optimal controls obtained for initial control in the grid \mathbf{u}_{ijk}^1 and for each case of the initial magnetic field \mathbf{v}_0 .



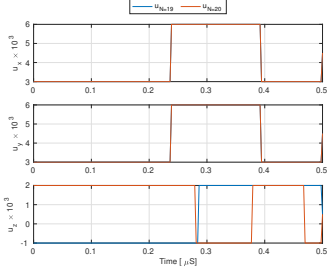
(a) Case $\mathbf{v}_0 = [6, 6, -1]\mu\text{T}$.



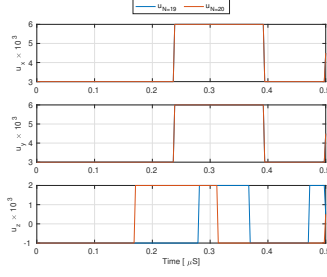
(b) Case $\mathbf{v}_0 = [6, 6, 2]\mu\text{T}$.

FIG. 16: 1-proton. Approximated optimal controls obtained for initial control in the grid \mathbf{u}_{ijk}^2 and for each case of the initial magnetic field \mathbf{v}_0 .

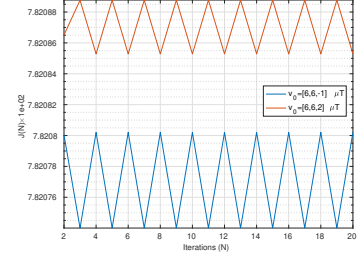
original non-filtered model with multiple bang-bang optimal magnetic fields and filtered model with continuous in time unique optimal magnetic field is associated with the loss of the maximum singlet yield expressed as a maximum of the cost functional within 1%. If the filtering parameter is chosen large, then the filtered model is close to the no-filter model and inherits the non-uniqueness of the optimal control.



(a) Case $\mathbf{v}_0 = [6, 6, -1]\mu T$.

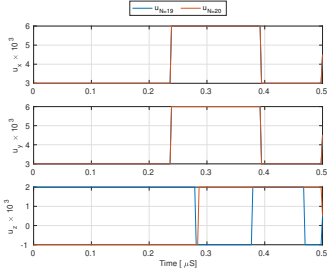


(b) Case $\mathbf{v}_0 = [6, 6, 2]\mu T$.

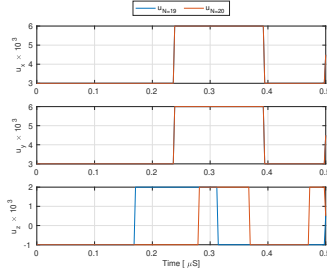


(c) Cost functional \mathcal{J} .

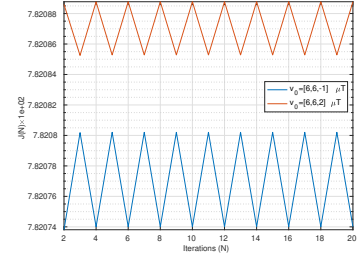
FIG. 17: 1-proton. Approximated bang-bang optimal control \mathbf{u}_{111} at iterations $N = 19$ and $N = 20$ for each case of \mathbf{v}_0 (left and center). Similar results were obtained for the remaining points of the grid \mathbf{u}_{ijk}^1 . Cost functional at each iteration and for each \mathbf{v}_0 case.



(a) Case $\mathbf{v}_0 = [6, 6, -1]\mu T$.



(b) Case $\mathbf{v}_0 = [6, 6, 2]\mu T$.



(c) Cost functional \mathcal{J} .

FIG. 18: 1-proton. Approximated bang-bang optimal control $\tilde{\mathbf{u}}_{111}$ at iterations $N = 19$ and $N = 20$ for each case of \mathbf{v}_0 (left and center). Similar results were obtained for the remaining points of the grid \mathbf{u}_{ijk}^2 . Cost functional at each iteration and for each \mathbf{v}_0 case.

VIII. CONCLUSIONS

We consider the quantum optimal control problem to devise the shape of the external electromagnetic field which drives the spin dynamics of radical pairs to quantum coherent state through maximization of the triplet-singlet yield in biochemical reactions. The mathematical model is a Schrödinger system with spin Hamiltonian given by the sum of Zeeman interaction and hyperfine coupling interaction terms. In a recent paper [32] we proved Pontryagin Maximum Principle and established a bang-bang structure of the optimal electromagnetic field intensity. The main goal of this paper is to develop a method to produce a simplest continuous in time electromagnetic wave input which is almost optimal

in the sense that it provides a quantum triplet-singlet yield with minimal loss of the optimal one corresponding to optimal bang-bang electromagnetic field input. We introduce a one-parameter family of optimal control problems by coupling the Schrödinger system to a control field through filtering equations for the electromagnetic field. The idea of filtering is to avoid the discontinuity of the optimal electromagnetic field intensity.

- Fréchet differentiability in Hilbert spaces is proved and the formula for the first-order Fréchet derivative is derived, and gradient projection method (GPM) in Hilbert space is developed. Pontryagin Maximum Principle (PMP) in Hilbert space is proved and the bang-bang structure of the optimal control is established. As an output of the filtering equation the optimal electromagnetic field input produced by PMP is continuous and piecewise smooth in time.
- A closed optimality system of nonlinear integro-differential equations for the identification of the bang-bang optimal control is revealed. A new two-step algorithm for the calculation of the bang-bang optimal control, called **explicit Pontryagin maximum principle** (EPMP) method is developed.
- Approximation of the EPMP method, so called **iterative Pontryagin maximum principle** (IPMP) method is developed. It consists of an iterative process of solving initial value problems for the Schrödinger system, and it's adjoined with subsequent derivation of the next iteration of the bang-bang optimal control via Pontryagin maximum principle.
- Software is developed and numerical simulations of up to 7-proton models are pursued implementing IPMP and GPM algorithms. It is demonstrated that if the electromagnetic field range has a fixed sign, IPMP and GPM methods converge to the unique bang-bang optimal control and produce the same unique continuous in time optimal electromagnetic field input. The simulations show that the IPMP method converges twice faster than GPM method in terms of number of iterations, which is especially apparent for higher proton models when computational cost increases exponentially.
- Numerical simulations of up to 7-proton models with filtering parameter range $0.1 \leq \gamma \leq 60$, and with various selection of initial iterations demonstrate that **trading off between the original non-filtered model with bang-bang optimal magnetic**

field and filtered model with continuous in time optimal magnetic field is associated with the loss of the maximum singlet yield expressed as a maximum of the cost functional within 1%. Hence, filtering presents a powerful regularization tool to replace optimal bang-bang electromagnetic field input with the continuous in time electromagnetic field wave which produces almost the same quantum singlet yield, and possibly preserves the quantum coherence of the radical pair system.

- Numerical simulations demonstrate that the best selection of filtering parameters γ and \mathbf{v}_0 in terms of minimal loss of quantum singlet yield is achieved by choosing γ large, and by selecting initial value of the magnetic field \mathbf{v}_0 to match the initial value of the optimal bang-bang magnetic field in no-filter model.
- In general, if the electromagnetic field range has a changing sign there is a non-uniqueness of the optimal control, and both IPMP and GPM methods demonstrate the local convergence and stability, due to non-uniqueness of the optimal control. IPMP has an advantage over GPM in terms of local convergence rate and efficiency.
- Filtering presents a powerful regularization tool to address the non-uniqueness of the optimal control in the original no-filter model. Numerical simulations demonstrate that by choosing the filtering parameter γ small enough, the filtered optimal control problem has a unique bang-bang optimal control. Moreover, **trading off between the original non-filtered model with multiple bang-bang optimal magnetic fields and filtered model with continuous in time unique optimal magnetic field is associated with the loss of the maximum singlet yield expressed as a maximum of the cost functional within 1%.**
- The results open a venue for a potential experimental work for the magnetoreception as a manifestation of quantum biological phenomena.

Data Availability Statement

Data were generated by the authors and included in the article. The datasets generated and/or analyzed during the current study are publicly available in the following repository:

https://gitlab.com/oist_proj/pmp_filtering.git.

ACKNOWLEDGMENTS

We are grateful for the help and support provided by the Scientific Computing and Data Analysis section of Core Facilities at OIST.

IX. REFERENCES

-
- [1] M. Bucci, C. Goodman, and T. L. Sheppard, A decade of chemical biology, *Nat. Chem. Biol.* **6**, 847 (2010).
 - [2] P. Ball, The dawn of quantum biology, *Nature* **9**, 10 (2011).
 - [3] N. Lambert and et al., Quantum biology, *Nat. Phys.* **9**, 10 (2013).
 - [4] T. Ritz and et al., Magnetic compass of birds is based on a molecule with optimal directional sensitivity, *Biophysical journal* **96**, 3451 (2009).
 - [5] T. Ritz, P. Thalau, J. B. Phillips, R. Wiltschko, and W. Wiltschko, Resonance effects indicate a radical-pair mechanism for avian magnetic compass, *Nature* **429**, 177 (2004).
 - [6] C. Niessner and et al., Magnetoreception: activated cryptochrome 1a concurs with magnetic orientation in birds, *Journal of the Royal Society, Interface* **10**, 20130638 (2013).
 - [7] R. J. Usselman, C. Chavarriaga, P. R. Castello, M. Procopio, T. Ritz, E. A. Dratz, D. J. Singel, and C. F. Martino, The quantum biology of reactive oxygen species partitioning impacts cellular bioenergetics, *Sci. Rep.* **6**, 38543 (2016).
 - [8] J. Cai, F. Caruso, and M. B. Plenio, Quantum limits for the magnetic sensitivity of a chemical compass, *Phys. Rev. A* **85**, 040304 (2012).
 - [9] J. Cai and M. B. Plenio, Chemical compass model for avian magnetoreception as a quantum coherent device, *Phys. Rev. Lett.* **111**, 230503 (2013).
 - [10] F. Cintolesi, T. Ritz, C. W. M. Kay, C. R. Timmel, and P. J. Hore, Anisotropic recombination of an immobilized photoinduced radical pair in a 50- μ T magnetic field: a model avian photomagnetoreceptor, *Chemical Physics* **294**, 385 (2003).

- [11] L. Turin, A Spectroscopic Mechanism for Primary Olfactory Reception, *Chemical Senses* **21**, 773 (1996).
- [12] L. Turin, E. M. C. Skoulakis, and A. P. Horsfield, Electron spin changes during general anesthesia in *Drosophila*, *Proceedings of the National Academy of Sciences* **111**, E3524 (2014).
- [13] M. Mohseni and *et. al.*, *Quantum Effects in Biology* (Cambridge University Press, 2014).
- [14] P. I. Sia, A. N. Luiten, T. M. Stace, J. P. M. Wood, and R. J. Casson, Quantum biology of the retina, *Clinical & Experimental Ophthalmology* **42**, 582 (2014).
- [15] F. Rieke and D. A. Baylor, Single-photon detection by rod cells of the retina, *Rev. Mod. Phys.* **70**, 1027 (1998).
- [16] J. N. Tinsley, M. I. Molodtsov, R. Prevedel, D. Wartmann, J. Espigulé-Pons, M. Lauwers, and A. Vaziri, Direct detection of a single photon by humans, *Nature Communications* **7**, 12172 (2016).
- [17] L. Zueva, T. Golubeva, E. Korneeva, O. Resto, M. Inyushin, I. Khmelinskii, and V. Makarov, Quantum mechanism of light energy propagation through an avian retina, *Journal of Photochemistry and Photobiology B: Biology* **197**, 111543 (2019).
- [18] A. Dodin and P. Brumer, Light-induced processes in nature: Coherences in the establishment of the nonequilibrium steady state in model retinal isomerization, *The Journal of Chemical Physics* **150**, 184304 (2019).
- [19] G. Palczewska, F. Vinberg, P. Stremplewski, M. P. Bircher, D. Salom, K. Komar, J. Zhang, M. Cascella, M. Wojtkowski, V. J. Kefalov, and K. Palczewski, Human infrared vision is triggered by two-photon chromophore isomerization, *Proceedings of the National Academy of Sciences* **111**, E5445 (2014).
- [20] R. Wiltschko and W. Wiltschko, The magnetite-based receptors in the beak of birds and their role in avian navigation, *Journal of Comparative Physiology A* **199**, 89 (2013).
- [21] J. Shaw, A. Boyd, M. House, R. Woodward, F. Mathes, G. Cowin, M. Saunders, and B. Baer, Magnetic particle-mediated magnetoreception, *Journal of The Royal Society Interface* **12**, 20150499 (2015).
- [22] R. Usselman, I. Hill, D. Singel, and C. Martino, Spin biochemistry modulates reactive oxygen species (ros) production by radio frequency magnetic fields, *PLoS ONE* **9**, e93065 (2014).
- [23] V. J. Thannickal and B. L. Fanburg, Reactive oxygen species in cell signaling, *American Journal of Physiology-Lung Cellular and Molecular Physiology* **279**, L1005 (2000).

- [24] M. M. Diehn, R. W. Cho, and *et.al.*, Association of reactive oxygen species levels and radiore-sistance in cancer stem cells, *Nature* **458**, 780 (2009).
- [25] T. Finkel, Signal transduction by reactive oxygen species, *J Cell Biol.* **194**, 7 (2011).
- [26] P. D. Ray, B. W. Huang, and Y. Tsuji, Reactive oxygen species (ros) homeostasis and redox regulation in cellular signaling, *Cell Signal* **24**, 981 (2012).
- [27] C. L. Bigarella, R. Liang, and S. Ghaffari, Stem cells and the impact of ros signaling, *Devel-opment* **141**, 4206 (2014).
- [28] U. E. Steiner and T. Ulrich, Magnetic field effects in chemical kinetics and related phenomena, *Chemical Reviews* **89**, 51 (1989).
- [29] H. Zadeh-Haghigi and C. Simon, Magnetic field effects in biology from the perspective of radical pair mechanism, *J R Soc Interface* **19(193)** (2022).
- [30] K. Schulten and P. G. Wolynes, Semiclassical description of electron spin motion in radicals including the effect of electron hopping, *The Journal of Chemical Physics* **68**, 3292 (2008).
- [31] C. F. Martino, P. Jimenez, M. Goldfarb, and U. G. Abdulla, Optimization of parameters in coherent spin dynamics of radical pairs in quantum biology, *PLOS ONE* **18**, 1 (2023).
- [32] U. G. Abdulla, C. Martino, J. Rodrigues, P. Jimenez, and C. Zhen, Bang-bang optimal control in coherent spin dynamics of radical pairs in quantum biology, *Quantum Sci. Tech.* **9**, 045022 (2024).
- [33] F. T. Chowdhury, M. C. J. Denton, D. C. Bonser, and D. R. Kattnig, Quantum control of radical-pair dynamics beyond time-local optimization, *PRX Quantum* **5**, 020303 (2024).
- [34] S. J. Glaser, U. Boscain, T. Calarco, C. P. Koch, W. Köckenberger, R. Kosloff, I. Kuprov, B. Luy, S. Schirmer, T. Schulte-Herbrüggen, D. Sugny, and F. K. Wilhelm, Training schrödinger’s cat: quantum optimal control, *The European Physical Journal D* **69**, 279 (2015).
- [35] C. P. Koch, U. Boscain, T. Calarco, G. Dirr, S. Filipp, S. J. Glaser, R. Kosloff, S. Montangero, T. Schulte-Herbrüggen, D. Sugny, and F. K. Wilhelm, Quantum optimal control in quantum technologies. strategic report on current status, visions and goals for research in europe, *EPJ Quantum Technology* **9**, 19 (2022).
- [36] G. Turinici and H. Rabitz, Quantum wavefunction controllability, *Chemical Physics* **267**, 1 (2001).
- [37] C. Brif, R. Chakrabarti, and H. Rabitz, Control of quantum phenomena: past, present and future, *New Journal of Physics* **12**, 075008 (2010).

- [38] U. Boscain, M. Sigalotti, and D. Sugny, Introduction to the Pontryagin maximum principle for quantum optimal control, *PRX Quantum* **2**, 030203 (2021).
- [39] N. Ofek, A. Petrenko, R. Heeres, P. Reinhold, Z. Leghtas, B. Vlastakis, Y. Liu, L. Frunzo, S. Girvin, L. Jiang, M. Mirrahimi, M. Devoret, and R. Schoelkopf, Extending the lifetime of a quantum bit with error correction in superconducting circuits, *Nature* **536**, 441 (2016).
- [40] M. Werninghaus, D. Egger, F. Roy, S. Machnes, F. Wilhelm, and S. Filipp, Leakage reduction in fast superconducting qubit gates via optimal control, *npj Quantum Information* **7** (2021).
- [41] A. Larrouy, S. Patsch, R. Richaud, J.-M. Raimond, B. M. C. Koch, and S. Gleyzes, Fast navigation in a large hilbert space using quantum optimal control, *Phys Rev X* **10** (2020).
- [42] A. Omran, H. Levine, A. Keesling, G. Semeghini, T. Wang, S. Ebadi, H. Bernien, A. Zibrov, H. Pichler, S. Choi, J. Cui, M. Rossignolo, P. Rembold, S. Montangero, T. Calarco, M. Endres, M. Greiner, V. Vuletic, and M. Lukin, Generation and manipulation of schrodinger cat in rydberg atom arrays, *Science* **365** (2019).
- [43] F. Borselli, M. Maiwoger, T. Zhang, P. Haslinger, V. Mukherjee, A. Negretti, S. Montanegro, T. Calarco, I. Mazets, M. Bonneau, and J. Schmiedmayer, Two-particle interference with double twin-atom beams, *Phys Rev Lett* **126** (2021).
- [44] C. Figgatt, A. Ostrander, N. Linke, K. Landsman, D. Zhu, D. Maslov, and C. Monroe, Parallel entangling operations on a universal ion-trap quantum computer, *Nature* **572**, 368 (2019).
- [45] L. Magrini, P. Rosenzweig, C. Bach, A. Deutschmann-Olek, S. Hofer, S. Hong, N. Kiesel, A. Kugi, and M. Aspelmeyer, Real-time optimal quantum control of mechanical motion at room temperature, *Nature* **595**, 373 (2021).
- [46] U. G. Abdullaev, Quasilinearization and inverse problems of nonlinear dynamics, *J. Optim. Theory Appl.* **85**, 509 (1995).
- [47] U. G. Abdullaev, Quasilinearization and inverse problems for nonlinear control systems, *J. Optim. Theory Appl.* **85**, 527 (1995).
- [48] U. G. Abdulla and R. Poteau, Identification of parameters in systems biology, *Math. Biosci.* **305**, 133 (2018).
- [49] U. G. Abdulla and R. Poteau, Identification of parameters for large-scale kinetic models, *J. Comput. Phys.* **429**, Paper No. 110026, 19 (2021).
- [50] M. Hirose and P. Cappellaro, Time-optimal control with finite bandwidth, *Quantum Information Processing* **17**, 1 (2018).

- [51] O. A. Ladyženskaja, V. A. Solonnikov, and N. N. Ural'ceva, *Linear and quasilinear equations of parabolic type*, Translations of Mathematical Monographs, Vol. Vol. 23 (American Mathematical Society, Providence, RI, 1968) pp. xi+648.
- [52] I. K. Kominis, Quantum zeno effect explains magnetic-sensitive radical-ion-pair reactions, *Phys. Rev. E* **80**, 056115 (2009).
- [53] M. Tiersch and H. J. Briegel, Decoherence in the chemical compass: the role of decoherence for avian magnetoreception, *Philosophical Transactions of the Royal Society A: Mathematical, Physical and Engineering Sciences* **370**, 4517 (2012).
- [54] J. Luo, Sensitivity enhancement of radical-pair magnetoreceptors as a result of spin decoherence, *The Journal of Chemical Physics* **160**, 074306 (2024).
- [55] V. S. Poonia, D. Saha, and S. Ganguly, State transitions and decoherence in the avian compass, *Phys. Rev. E* **91**, 052709 (2015).
- [56] S. Worster, D. R. Kattnig, and P. J. Hore, Spin relaxation of radicals in cryptochrome and its role in avian magnetoreception, *The Journal of Chemical Physics* **145**, 035104 (2016).
- [57] T. P. Fay, L. P. Lindoy, and D. E. Manolopoulos, Spin relaxation in radical pairs from the stochastic Schrödinger equation, *The Journal of Chemical Physics* **154**, 084121 (2021).